# *In situ* growth and crystallization of $TiO_2$ on polymeric membranes for the photocatalytic degradation of diclofenac and 17α-ethinylestradiol

Seghir Dekkouche[1,2], Sergio Morales-Torres[3,*], Ana R. Ribeiro[2], Joaquim L. Faria[2], Clàudia Fontàs[4], Ounissa Kebiche-Senhadji[1], Adrián M.T. Silva[2,*]

[1]*Laboratoire des Procédés Membranaires et des Techniques de Séparation et de Récupération (LPMTSR), Faculté de Technologie, Université de Bejaia, 06000 Bejaia, Algérie.*

[2]*Laboratory of Separation and Reaction Engineering - Laboratory of Catalysis and Materials (LSRE-LCM), Faculdade de Engenharia, Universidade do Porto, Rua Dr. Roberto Frias s/n, 4200-465 Porto, Portugal.*

[3]*Department of Inorganic Chemistry, Faculty of Sciences, University of Granada, Campus Fuentenueva s/n, ES-18071 Granada, Spain.*

[4]*Department of Chemistry, University of Girona, C/Maria Aurèlia Capmany 69,17003 Girona, Spain.*

***Corresponding authors: semoto@ugr.es (S. Morales-Torres), adrian@fe.up.pt (A.M.T. Silva).***

## Abstract

$TiO_2$ *in situ* growth on three commercial membranes (polysulfone, polyvinylidene fluoride –PVDF and polytetrafluoroethylene –PTFE) and its hydrothermal post-crystallization to transform $TiO_2$ into a photocatalytically-active phase, were investigated under mild synthesis conditions to preserve the textural properties of the supports. The membranes were successfully prepared and characterized by scanning electron microscopy, thermogravimetry analysis, $N_2$ physisorption, X-ray diffraction, and water contact angle measurements, among other techniques. Membrane supports with a more opened porosity and high hydrophilicity allowed to enhance the content and distribution of the anatase $TiO_2$ nanoparticles on the membrane surface. The efficiency and the permeate flux of the developed membranes were investigated to simultaneously remove diclofenac (DCF) and 17α-ethinylestradiol (EE2) from water by adsorption and UV–LED (light-emitting diode) photocatalysis under continuous recirculating mode. All $TiO_2$ membranes achieved removal efficiencies above 90 % for both contaminants, EE2 being always preferentially adsorbed over DCF due to electrostatic repulsions between the DCF molecules and the surface of these membranes. The permeate flux of $TiO_2$ membranes was enhanced after UV-LED exposure as a consequence of the degradation of the contaminants adsorbed on the membrane surface during the dark phase. Moreover, the stability of $TiO_2$ nanoparticles on these membranes was studied by static tests under sonication and several consecutive reaction cycles. The $TiO_2$ membrane prepared with PVDF was the most stable, also presenting a high photocatalytic activity.

***Keywords:*** *heterogeneous photocatalysis; polymeric membranes; filtration; pharmaceuticals; water treatment.*

## 1. Introduction

The production of pharmaceuticals has considerably increased worldwide in the last decades, including hormones, anti-inflammatories, antiepileptics, antidepressants, antibiotics, among others [1]. Humans and animals consume these compounds, metabolize them and excrete through urine and feces, reaching wastewater treatment plants (WWTPs) [1-3]. Conventional municipal and urban WWTPs are not designed to eliminate these organic micropollutants [4-6] at trace concentrations, which accumulate in surface and ground waters, and appear even in drinking water [1, 2, 4].

Diclofenac (DCF) and 17α-ethinylestradiol (EE2) were included in the Watch List of substances for European Union-wide monitoring to support future prioritization exercises in the Decision 2015/495/EU of 20 March 2015, which current version is Decision 2020/1161 of 4 August 2020 [7]. DCF is a non-steroidal anti-inflammatory drug prescribed to treat chronic rheumatism, migraines, fever, and muscle pain [8, 9] At the same time, EE2 is a synthetic steroid hormone administered as an oral contraceptive to treat prostate, breast cancer, and alopecia (in hair lotions) [9, 10]. The detection of both DCF and EE2 at very low concentrations (ng $L^{-1}$) in different water matrices has been widely described in the literature [11-13]. Even at low concentrations, DCF and EE2 can cause cardiovascular complications [9] and negatively influence the reproduction of specific fish species [12], respectively.

Advanced oxidation processes (AOPs) are an alternative option for the degradation of these persistent micropollutants in WWTPs through the generation of hydroxyl radicals (•OH) [14], which are extraordinarily reactive species able to attack most of the organic molecules with rate constants usually in the order of $10^6 – 10^9$ $M^{-1}$ $s^{-1}$ [15]. Among different AOPs, there is a claimed interest in heterogeneous photocatalysis as a water treatment technology. $TiO_2$ is the most widely employed photocatalyst due to its low cost, low toxicity, good chemical and thermal stability, and high photo-activity under UV irradiation [16-18]. The degradation of

several micropollutants by the hydroxyl radicals generated from the water oxidation through valence band holes and reducing dissolved oxygen by the excited electrons under UV irradiation of the catalyst has been reported [14, 19, 20]. Furthermore, for the XXI century energy transition requirement, the use of economic light sources is the panacea of the future – LED sources are at the forefront of any type of application, either consumer-oriented or industrial applied.

Photocatalysts are often employed as suspended particles (i.e., slurries) in water [8, 16, 21-23], requiring an additional treatment step for the material retrieval, which may be difficult due to the high dispersion of the catalyst nanoparticles in the reaction medium. In recent years, hybrid systems based on integrating AOPs with membrane technologies have been studied to overcome this limitation. These integrated hybrid systems are known as photocatalytic membrane reactors (PMRs), and are mainly implemented as two strategies: (i) the photocatalyst immobilized onto/into the membrane, or (ii) a configuration with the photocatalyst suspended in water and a membrane acting as a physical barrier for the photocatalyst nanoparticles and contaminants [24-26]. The second system is the most common, but it is also prone to membrane fouling originated by organic pollutants, catalyst particles, and other substances. Thus, the immobilization of photocatalysts into/onto membranes has been investigated to mitigate the fouling and achieve high fluxes [27-32]. Furthermore, in this case, the membrane acts simultaneously as catalyst support, selective barrier, and adsorbent for the substances to be removed. Therefore, the pollutant photodegradation takes place in one-step, saving energy, time and space.

Nonetheless, photocatalytic membranes present some drawbacks such as possible photocatalyst leaching, a reduced surface accessible to the irradiation and the pollutants, and a structure susceptible to be damaged by the irradiation and the reactive oxygen species, in particular when polymeric membranes are employed instead of ceramic ones [29, 33, 34]. These limitations can

be circumvented by improving the porosity and binding the photocatalyst to the membrane by specific synthesis methods [29], and controlling the size, dispersion, and crystalline phase of the photocatalyst into/onto membranes. In fact, concerning the resistance to UV irradiation and the oxidative environment, ceramic membranes are more resistant than polymeric ones [35], but they are also more expensive and complex to be fabricated. In the case of polymeric membranes, the catalyst can be deposited onto the membrane acting as a protective skin [31], or they can be fabricated by using polymers such as polyvinylidene fluoride (PVDF) and polytetrafluoroethylene (PTFE), which have demonstrated an excellent resistance under UV and UV/$H_2O_2$ [35]. Even so, there are still some challenges for the practical application, in either case, membrane stability being one of them. New membrane compositions with superior chemical stability and better mechanical strength are sought. In this context, the application of PMRs for degradation of pharmaceuticals [28, 36] or other organic pollutants [27, 37, 38] in water has been studied, but only a few works were found for DCF [39-42] and EE2 [43-45].

In this study, we investigate three typical hydrophilic membranes, i.e., PTFE, PVDF and polysulfone (PS), as $TiO_2$ support for the simultaneous removal of DCF and EE2 in water under UV–LED (light-emitting diode) irradiation. Microfiltration membranes were selected due to the low operating pressure and energy consumption required compared to nanofiltration or reverse osmosis membranes. $TiO_2$ membranes were developed by a two-step method, which includes *in situ* growing of $TiO_2$ on the polymer structure and its post-crystallization by a hydrothermal treatment. The structure and hydrophilicity of the $TiO_2$ membranes and neat membranes used as reference were studied by different techniques. The efficiency for the removal of both pollutants was assessed by adsorption and photocatalytic experiments under continuous recirculating mode. A special attention is given to the membrane fouling and stability for long-term operation in order to develop practical approaches for reducing this problem.

## 2. Experimental

### *2.1. Materials*

PVDF and PTFE membranes acquired from Merck Millipore and PS membranes purchased from Pall Corporation were used as supports of the $TiO_2$ particles. Some properties of these commercial membranes are summarized in Table 1. Absolute ethanol ($C_2H_5OH$, ≥ 99 %) from Valente e Ribeiro Lda. and titanium (IV) isopropoxide (TTIP, ≥97 %) from Sigma-Aldrich were used during the membrane synthesis. Sodium diclofenac salt, $C_{14}H_{10}Cl_2NNaO_2$, (DCF, ≥ 98 %) acquired from Cayman Chemical and 17α-ethinylestradiol, $C_{20}H_{24}O_2$, (EE2, ≥ 98 %) from Sigma-Aldrich were selected as model pollutants. Ultrapure water (resistivity = 18 mΩ $cm^{-1}$) was supplied by a Milli-Q water system.

**Table 1.** Structural properties and labels of commercial membranes provided by the manufacturers.

| **Nomenclature** | **PS** | **PTFE** | **PVDF** |
|---|---|---|---|
| Polymer | Polysulfone | Polytetrafluoroethylene | Polyvinylidene fluoride |
| Membrane | HT Tuffryn® | JGWP Omnipore® | GVWP Durapore® |
| Diameter (mm) | 25 | 25 | 25 |
| Pore size (μm) | 0.2 | 0.2 | 0.22 |
| Thickness (μm) | 163 | 65 | 110 |
| Bubble point (bar) | 3.5 | 13.6 | ≥ 3.5 |
| Water permeability (L $h^{-1}$ $m^{-2}$ $Pa^{-1}$) | 0.022 | 0.100 | n.p. |

*n.p. = not provided.

### 2.2. *Development of photocatalytic membranes*

PS, PVDF and PTFE membranes were used to prepare the corresponding photoactive membranes following a sol–gel methodology adapted from elsewhere [28]. In a typical synthesis procedure, the membrane support was previously activated by soaking in absolute ethanol for 30 s, then in an aqueous alcoholic solution (1:1) for 1 min and finally, in ultrapure water for 2 min. After that, the excess of solvent on the membrane surface was removed and then, it was soaked in an ethanolic solution containing 2 mmol $L^{-1}$ TTIP under moderate stirring for 2 h, the TTIP hydrolysis taking place directly on the wetted membrane surface. The resulting $TiO_2$ membranes were rinsed several times with ultrapure water and air-dried overnight. In a second step, the crystallization of the $TiO_2$ membranes was carried out by hydrothermal treatment with vapor in a Teflon-lined stainless-steel autoclave (Parr Instruments, USA Mod. 4748) using ultrapure water at 110 °C for 2 h, and finally, stored prior to use. The $TiO_2$ membranes were labelled as T–PS, T–PVDF and T–PTFE, indicating the membrane support used, i.e., PS, PVDF and PTFE, respectively. Neat membranes referred as N–PS, N–PVDF and N–PTFE were also tested for comparison purposes.

### 2.3. *Characterization techniques*

The morphology of the membranes was examined by scanning electron microscopy (SEM) using a FEI Quanta 400FEG ESEM/EDAX Genesis X4M instrument (accelerating voltage of 15 kV and a working distance of ca. 10–15 mm). For cross-section observations, the membranes were frozen and broken under liquid nitrogen. The amount of $TiO_2$ assembled on the polymeric membranes was quantified by thermogravimetric analysis (TGA), following a methodology adapted from the literature [46], the amount of $TiO_2$ being determined as the mass of the residue resulting from the complete decomposition of the polymer. TGA was performed in a STA 490 PC/4/H Luxx Netzsch thermal analyzer, by heating the membrane in air from 50 ºC to 900 ºC at 20 ºC $min^{-1}$. $N_2$ adsorption-desorption isotherms at –196 ºC were obtained in a

Quantachrome autosorb-iQ2 instrument. The apparent surface area ($S_{BET}$) was determined by applying the Brunauer–Emmett-Teller (BET) equation [47]. The volume of $N_2$ adsorbed at a relative pressure of 0.95 ($V_{pore}$) was obtained from the adsorption isotherms, which corresponds to the sum of the micro- and mesopore volumes according to Gurvitch's rule [46, 48]. The overall porosity ($\varepsilon$) of the membranes was determined by the gravimetric method described in detail elsewhere [49]. The densities for the PS, PVDF and PTFE polymers were 1.24, 1.78 and 2.20 g $cm^{-3}$, respectively [31, 50]. X-ray diffraction (XRD) analysis was performed in a PANalyticalX'Pert MPD equipped with an X'Celerator detector and secondary monochromator (Cu Kα λ = 0.154 nm, 50 kV, 40 mA). Rietveld refinement with a PowderCell software was applied for identification of the crystallographic phases, and the average crystal size ($d_{TiO2}$) was determined using the Scherrer equation. Fourier–transform infrared spectroscopy (FTIR) was performed in the range of 4000–600 $cm^{-1}$ using a Thermo Scientific™ Nicolet™ iS5 ATR–FTIR Spectrometer. The surface hydrophobicity of the membranes was studied by water contact angle measurements using an Attension® Theta optical tensiometer that allowed image acquisition and data analysis [50]. The measurements were carried out at room temperature, using the sessile drop method. Each contact angle was measured at least in 5 different locations on the dried membranes in order to determine an average value.

### *2.4. Stability tests of $TiO_2$ membranes*

The binding of $TiO_2$ nanoparticles to the membranes was studied by stability tests performed in an ultrasonication bath (P Selecta). In a typical test, the $TiO_2$ membrane was soaked in a glass baker containing 25 mL of ultrapure water, which was placed in an ultrasonication bath for 30 min and 40 Hz of amplitude. Aliquots were periodically withdrawn at different time intervals to monitor the amount of $TiO_2$ leached by UV-Vis spectrophotometry at 326 nm in a Jasco V-560 spectrophotometer by using a reference calibration curve (*absorbance = 0.036 × [$TiO_2$ in mg $L^{-1}$]*) that was obtained by considering the study published by J. Stötzel *et al.* [51]. These

authors found that at a selected wavelength, the absorbance increases with the concentration of $TiO_2$ nanoparticles suspended in an alcoholic solution of TTIP during hydrolysis.

### *2.5. Evaluation of membrane performance*

The photocatalytic efficiency of the membranes was evaluated under UV–LED irradiation in a lab-scale setup (Fig. 1). The membrane was placed into a "U–shaped" borosilicate glass cylindrical reactor (effective area of 2.27 $cm^2$) operating in dead-end filtration mode at room temperature. A reservoir containing 100 mL of an aqueous solution containing DCF (1.01 μmol $L^{-1}$) and EE2 (1.01 μmol $L^{-1}$) was magnetically stirred and continuously purged with air flow. The selected concentrations of EE2 and DCF (1.01 μmol $L^{-1}$) correspond to mass concentrations in the ppb level (specifically 300 μg $L^{-1}$) to mimic the actual concentrations of these micropollutants (ng $L^{-1}$) in some wastewaters, while assuring that the limits of detection (0.21 and 0.3 μg $L^{-1}$ for EE2 and DCF, respectively) and quantification (0.64 and 0.91 μg $L^{-1}$ for EE2 and DCF, respectively) of the method for these pollutants allowed to quantify removals close to 100 %.

In a typical run, the spiked solution was continuously pumped through the membrane reactor in continuous recirculating mode at a flow rate of 5 mL $min^{-1}$ under dark conditions for 24 h. The irradiation was performed using a 10 W high-intensity UV–LED (15.5 mm × 23 mm) emitting at 395 nm, located outside symmetrically at 4 cm from the membrane placed in the photoreactor, whereas diclofenac absorbs up to *ca.* 325 nm and thus photolysis is not likely to occur in this system [52]. The average nominal irradiance of UV–LED was 450 W $m^{-2}$ determined taking into account the reactor encasing and using a UV–vis spectroradiometer (OceanOptics USB2000+). During the adsorption and reaction stages (48 h), small aliquots (1.0 mL) were periodically withdrawn from the reservoir at different time intervals to monitor the concentrations of pollutants by High Performance Liquid Chromatography (HPLC), using a Shimadzu Corporation apparatus equipped with a fluorescence detector (RF-20AXS). A

Kinetex™ XB-C18 100 Å column (100 × 2.1 mm i.d.; 1.7 µm particle diameter) supplied by Phenomenex, Inc. (California, USA) was employed. The temperature of the column oven and autosampler were set at 40 °C and 15 °C, respectively, while the injection volume was 20 µL. The mobile phase consisted of a mixture of 0.1 % formic acid and acetonitrile (50:50 v/v) at isocratic mode, with a flow rate of 0.20 mL $min^{-1}$. The excitation wavelength of the fluorescence detector was 285 nm, while the emission wavelength was 310 nm in the first 4.5 min of the chromatographic run and 360 nm from 4.5 until the end of the run (8.0 min). Blank experiments were also performed with neat membranes to evaluate the direct photolysis and the filtration capacity of the membranes.

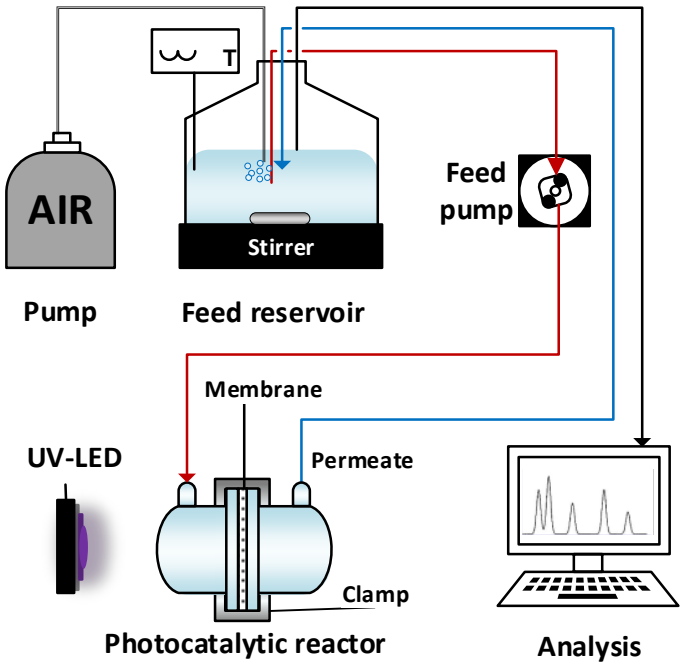


**Fig. 1.** Schematic diagram of the photocatalytic lab-scale setup.

The permeate flux (L $m^{-2}$ $h^{-1}$, LMH) was calculated according to the following equation:

$$F = \frac{V}{A\,x\,t} \quad (1)$$

where $V$ (L) is the volume of the solution permeated during the experiment, $A$ represents the effective membrane area ($m^2$), and $t$ denotes time (h).

## 3. Results and discussion

### *3.1. Membrane characterization and stability*

The top surface and cross-section of the different neat and $TiO_2$ membranes were studied by SEM (Fig. 2). As expected, the morphology of the neat membranes is markedly affected by the type of polymer and the fabrication method. Thus, N–PS shows a smooth surface formed by spherical-like pores resulting from polysulfone precipitation during its fabrication (Fig. 2a), while N–PTFE and N–PVDF membranes present a more opened structure formed by polymer fibers (Fig. 2d) or sheets (Fig. 2g), respectively. In general, a denser surface was observed for all $TiO_2$ membranes (Figs. 2b-c, 2e-f and 2h-i) compared to their corresponding neat membranes, as consequence of an ultra-thin layer of $TiO_2$ nanoparticles successfully assembled on the membrane surface through the proposed sol-gel method. For instance, it is clearly observed that pores become narrower in T–PS than those observed in N–PS (Fig. 2b *vs*. 2a, respectively). The largest $TiO_2$ content seems to be achieved for T–PS (Fig. 2c), which is homogenously deposited as particle clusters throughout the membrane surface. On the contrary, these characterization results suggest that T–PTFE and T–PVDF have lower amounts of $TiO_2$ nanoparticles, which were preferably self-assembled on the outer wall of the PTFE fibers (Fig. 2f) or surface of PVDF sheets, respectively (Fig. 2i). These differences observed in the location and content of $TiO_2$ should be related with the support properties and synthesis procedure used in membranes, which pursues the direct hydrolysis of the titanium precursor *in situ* on the membrane surface [28]. Thus, the dense structure of N–PS and its reactive sulfone groups and ether bonds favour, via coordination with $Ti^{4+}$ and H-bonds with hydroxyl groups of $TiO_2$, a significant attachment of $TiO_2$ particles on the surface of the membrane [53], while $TiO_2$ is self-assembled on the different opened structures of N–PTFE and N–PVDF by physical bonds due to the absence of these sulfone groups on their surfaces (Fig. 3) [54]. EDS spectra for selected

areas of each membrane confirmed the growth and formation of $TiO_2$ particles on the membrane (Fig. 2).

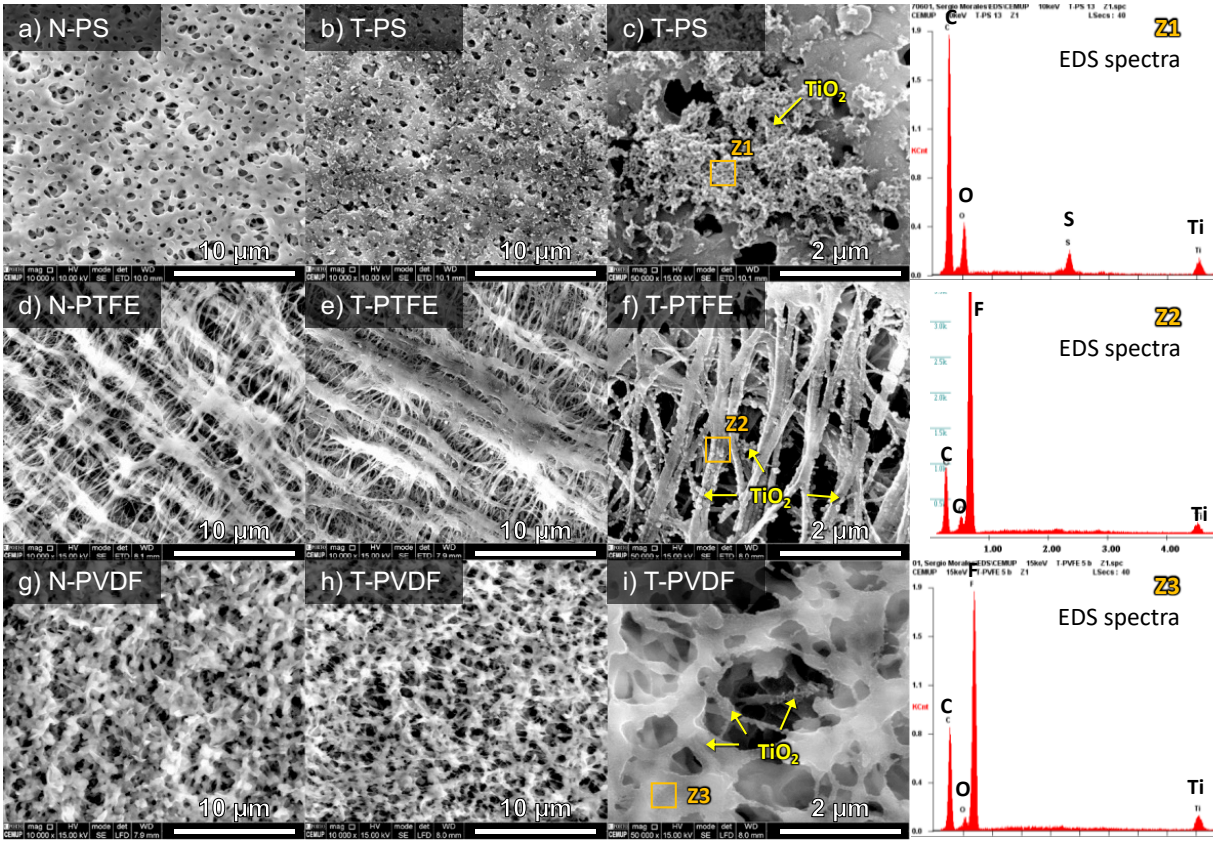


**Fig. 2.** SEM micrographs at different magnifications of the top surface for neat and $TiO_2$ membranes prepared over (a-c) PS, (d-f) PTFE and (g-i) PVDF supports. EDS spectra of selected areas are also included as reference.

Cross-sectional images of neat and $TiO_2$ membranes with PS and PVDF supports (Figs. S1a-c and 4d-f of the supporting information, respectively) corroborate that an ultra-thin layer of the $TiO_2$ material was homogeneously deposited on the corresponding membrane without the significant presence of cracks, voids or other defects, even if considered that these membranes were fractured for SEM analysis. PTFE membranes were difficult to fracture for accurate SEM analysis due to the high thermal resistance of this polymer. Both N–PS and N–PVDF membranes presented a symmetric structure (Fig. S1a-b and S1d-e, respectively), which is usual in commercial membranes. In general, $TiO_2$ seems well-assembled only on the top surface for

T–PS (Fig. S1c), while some particles on the PVDF sheets are observed across the membrane (Fig. S1f). Therefore, the synthesis method used to prepare the $TiO_2$ membranes allowed the formation of an ultra-thin layer of $TiO_2$ well-assembled to the membrane support, which is crucial to improve the stability in aqueous solution under steady-state flow. For instance, $TiO_2$ membranes prepared by other methods such as dip-coating or vacuum filtering were not effective enough during consecutive reaction cycles or long reaction periods [31, 55].

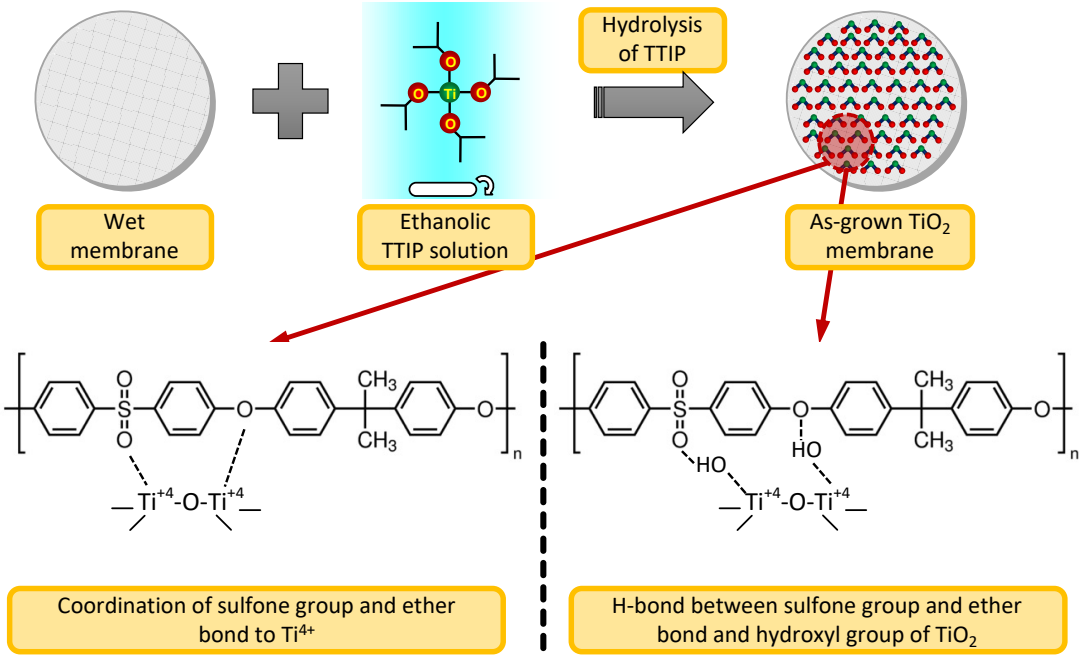


**Fig. 3.** Schematic representation of the interaction between the PS polymer structure and $TiO_2$.

The amount of $TiO_2$ in the corresponding membranes was determined by TGA under air atmosphere (Table 2). The $TiO_2$ content incorporated in membranes decreased as follows: T–PS > T–PVDF > T–PTFE, in agreement with SEM observations. Thus, the dense structure and the sulfone groups of the PS membrane allows to assemble more $TiO_2$ (i.e., 11.0 wt.%) than the other supports (i.e., 2.7 and 3.3 wt.% for T–PTFE and T–PVDF, respectively). Fig. 4 shows the TG curves obtained for neat and $TiO_2$ membranes. The temperature decomposition of the membrane depends on the type of polymer used during its fabrication. Thus, N–PS decomposed at 645 ºC, followed by N–PTFE (585 ºC) and finally, N–PVDF (551 ºC). For N–PS and N–

PVDF, another weight loss at a lower temperature (i.e., 532 and 481 ºC, respectively) was observed and it may be ascribed to the decomposition of a co–polymer or additive added during their fabrication. For instance, polyvinylpyrrolidone (PVP) is commonly used as pore former agent [49]. For the case of $TiO_2$ membranes, different behaviours were observed depending on the selected membrane support. Thus, the decomposition polymer increased up to 665 ºC for T–PS, while it was comparable for T–PTFE and T–PVDF (i.e., 580 and 546 ºC, respectively). It is well-known that the incorporation of surface modifiers or fillers in membranes may improve their thermal stability [49, 50]. In our case, $TiO_2$ is directly assembled on the polymeric matrix, protecting the polymer from decomposition and improving the thermal stability of membranes, in particular when incorporated in larger amounts (i.e., T–PS).

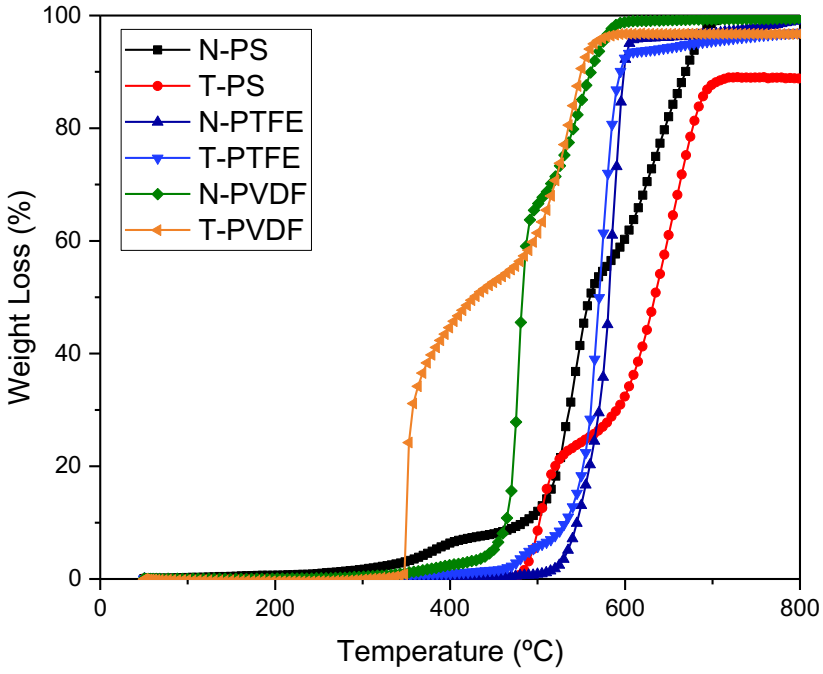


**Fig. 4.** TG curves obtained under air atmosphere of neat (uncoated) and $TiO_2$ membranes.

The textural properties of all membranes were studied by measurements of overall porosity ($\varepsilon$) and $N_2$ physisorption at –196 ºC. In general, the porosity of the commercial supports was higher than ~60 %, N–PS being the most porous membrane (Table 2). The assembly of $TiO_2$ particles

on the membranes only produced an evident decrease of porosity for T–PS, since that for T–PTFE and T–PVDF was comparable to their corresponding commercial supports (e.g., $\varepsilon$ = ~63 and ~59 % for N–PTFE and T–PTFE, respectively). This fact could be due to an important pore blockage by $TiO_2$-particle clusters on T–PS membrane. The formation of these clusters could have been formed during the TTIP hydrolysis and favoured by the highest porosity of N–PS.

Nitrogen adsorption-desorption isotherms for all membranes were analysed and gathered in Fig. S2 of the supporting information. In general, all adsorption isotherms can be considered of type–II, in accordance with IUPAC classification, typical of macroporous materials or materials with low porosity [14]. In fact, all membranes practically did not possess volume of $N_2$ adsorbed at low relative pressures, which is indicative of the absence of micropores filling. On the contrary, the volume adsorbed at high relative pressures quickly increases due to the filling of mesopores, which are responsible for the appearance of a hysteresis loop (Fig. S2). From adsorption data, the apparent BET surface area ($S_{BET}$) and the pore volume ($V_{pore}$) were determined (Table 2). All neat membranes presented low $S_{BET}$ values (i.e., 20–51 $m^2\ g^{-1}$), which are explained by the absence of micropores. Among the commercial supports, N–PTFE presented the highest $S_{BET}$ (i.e., 51 $m^2\ g^{-1}$) due to the largest $V_{pore}$ (i.e., 0.10 $cm^3\ g^{-1}$). When $TiO_2$ was deposited on these membranes, the surface area was enhanced regardless of the type of membrane used (e.g., 51 and 71 $m^2\ g^{-1}$ for N–PTFE and T–PTFE, respectively). It is noteworthy that T–PS presented a ~2.5-folds $S_{BET}$ compared to the neat PS membrane, although its overall porosity was lower (Table 2). This fact should be due to the largest amount of $TiO_2$ incorporated, which is a porous material and provides an improvement of the textural properties when assembled on the membrane surface. Among $TiO_2$ membranes, the $S_{BET}$ decreased as follows: T–PTFE > T–PVDF > T–PS; and thereby, the $TiO_2$ assembly on PTFE fibers and PVDF sheets is preferred to obtain membranes with better textural properties. Taking into account the results obtained by the gravimetric and $N_2$ physisorption methods, the two-step

method to synthetize the $TiO_2$ membranes seems to be adequate to obtain porous membranes, since the small variations in porosity should be ascribed to the pore blockage by $TiO_2$ that damages the polymeric structure produced during the TTIP hydrolysis or post-crystallization.

**Table 2.** Characterization of the membranes.

| Membrane | *$TiO_2$ (wt.%) | $\varepsilon$ (%) | $S_{BET}$ ($m^2\ g^{-1}$) | $V_{pore}$ ($cm^3\ g^{-1}$) | $d_{TiO2}$ (nm) | Contact angle ($\theta$°) |
|---|---|---|---|---|---|---|
| N–PS | 0.0 | 71 ± 1 | 20 | 0.03 | – | 56 ± 1 |
| N–PTFE | 0.0 | 63 ± 1 | 51 | 0.10 | – | 91 ± 1 |
| N–PVDF | 0.0 | 60 ± 1 | 30 | 0.04 | – | 80 ± 2 |
| T–PS | 11.0 | 35 ± 1 | 46 | 0.09 | 8.9 ± 1.1 | 26 ± 1 |
| T–PTFE | 2.7 | 59 ± 1 | 71 | 0.13 | 7.0 ± 1.0 | 86 ± 1 |
| T–PVDF | 3.3 | 59 ± 1 | 56 | 0.11 | 6.6 ± 1.0 | 76 ± 1 |

*Amount of $TiO_2$ on membranes determined by TGA; ε = porosity by gravimetric method; $S_{BET}$ and $V_{pore}$ estimated from $N_2$ physisorption data at –196 ºC; $d_{TiO2}$ = average crystallite size determined from XRD patterns.

After $TiO_2$ growth on membranes without crystallization, $TiO_2$ was amorphous as corroborated by the absence of peaks in the corresponding XRD pattern shown in Fig. 5. Thus, a crystallization process was performed to transform amorphous $TiO_2$ particles into a photocatalytically-active phase, like anatase [28, 56], since different studies reported the less photoactivity of amorphous $TiO_2$ nanoparticles compared to those in the crystalline form [57]. The crystallization of $TiO_2$ is usually performed by calcination at temperatures exceeding 500 ºC [17], but this pre-treatment is not suitable taking into account the thermal sensitive characteristics of the selected polymeric supports (Fig. 4). A strategy to crystallize $TiO_2$ at mild conditions consists in the hydrothermal treatment with *in situ* vapor generated. Thus, $TiO_2$ membranes were hydrothermally treated with vapor. XRD patterns of the crystallized

membranes clearly showed the presence of anatase (JCPDS Card no. 21–1272) with peaks placed at $2\theta$ values of 25.3º, 36.8º, 47.6º, 54.2º, 56.3º, 62.4º and 69.1, which correspond to (101), (004), (200), (105), (211), (204) and (116) crystal planes. This crystallization method is based on the adsorption of water vapor on the amorphous $TiO_2$, leading to the rearrangement of $TiO_6^{2-}$ octahedral units and leading to the formation of anatase crystallites [56]. The peaks placed at 28.7º and 31.7º for T–PTFE should be ascribed to the commercial PTFE support [58]. On the other hand, the average crystal size ($d_{TiO2}$) for $TiO_2$ membranes was obtained from diffraction patterns using the Debye–Scherrer equation (Table 2). In general, the crystallite sizes determined were small in the range of ~6.5 – 9.0 nm with no large differences for the different $TiO_2$ membranes, although slightly lower values were obtained for T–PTFE and T–PVDF. Therefore, the hydrothermal treatment with vapor was effective to form small $TiO_2$ crystallites of anatase and to preserve the textural properties of the membranes.

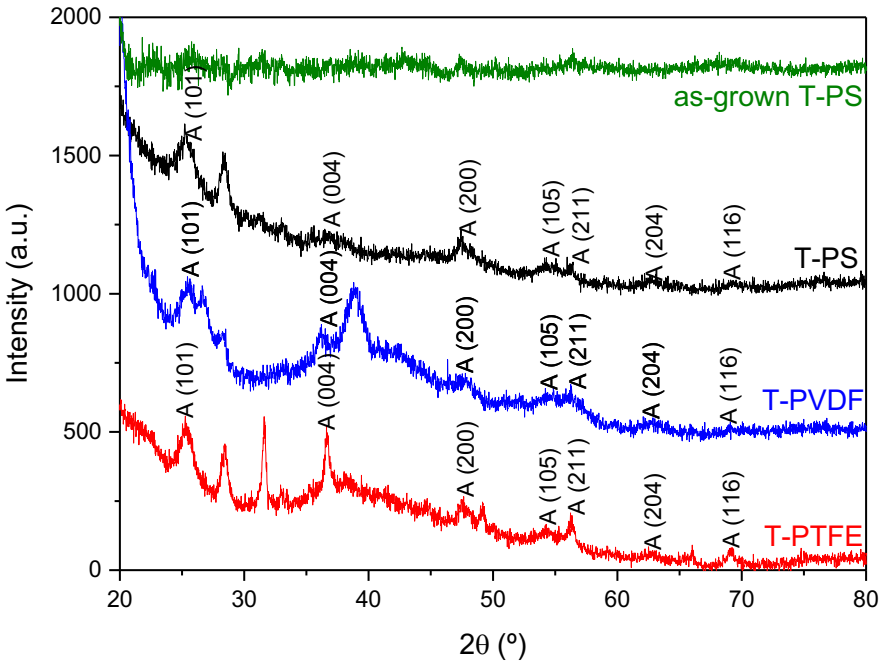


**Fig. 5.** XRD patterns of $TiO_2$ membranes prepared on PS, PVDF and PTFE supports. The as-grown T–PS (without crystallization) was also included for comparison.

ATR-FTIR spectra for $TiO_2$, neat and $TiO_2$ membranes (fresh and spent) are shown in Fig. S3 of the supporting information. Regarding Fig. S2a (bare $TiO_2$), the broad bands at high wavenumbers (3700–3000 $cm^{-1}$) can be ascribed to the stretching vibration of hydroxyl groups (O–H), as a consequence of the high affinity of $TiO_2$ nanoparticles to water molecules [59]. The band at 1643 $cm^{-1}$ is related to the stretching vibration of O–H bending of Ti–OH [60, 61], whereas low–intensity peaks between 1500 and 875 $cm^{-1}$ can be attributed to the lattice vibration of $TiO_2$ [62]. In the range of 1000–600 $cm^{-1}$, the peaks can be assigned to Ti–O, O–Ti–O and Ti–O–Ti [38, 63]. Concerning the N–PS membrane (Fig. S3b), some peaks relative to O–H in the range of 3700–3200 $cm^{-1}$ were observed from the possible interactions between C=C (in aromatic rings of PS) and water [64]. The peaks appearing at 3161, 3053, 1020 and 838 $cm^{-1}$, and those at 2960 and 2886 $cm^{-1}$ can be assigned to the stretching vibration of C–H of the aromatic rings, and alkanes, respectively, in the structure of PS [65, 66]. The aromatic links appeared also at 1582 and 1490 $cm^{-1}$ [35]. Asymmetrical and symmetrical stretching vibration of sulfone groups (S=O), and stretching vibration of ether groups (C–O–C), can be also observed at 1308 and 1154 $cm^{-1}$, and at 1238 $cm^{-1}$, respectively [67]. Comparing the ATR–FTIR spectrum of T–PS–Fresh to that of N–PS (Fig. S3b), some clear differences are observed. For instance, the bands between 3500 and 3000 $cm^{-1}$ and at 1643 $cm^{-1}$ in the T–PS–Fresh spectrum are more similar to those observed for bare $TiO_2$ (Fig. S3a) than for N–PS (Fig. S3b), which can be associated to surface hydroxyl groups and to water moisture. Moreover, the T–PS–Fresh spectrum has more intense bands at wavenumbers of <1000 $cm^{-1}$, corresponding to strong $TiO_2$ modes (Fig. S3a), these observations confirming the presence $TiO_2$ in the PS structure. However, differences were not observed when the ATR–FTIR spectra of spent and fresh membranes are compared. In general, these conclusions were quite similar for the other membranes under study (Fig. S3c and d). As additional information, regarding the ATR–FTIR spectra of N–PTFE and T–PTFE–Fresh (Fig. S3c), the characteristic peaks of N-PTFE at 1444

$cm^{-1}$ ($CF_2$ combined asymmetric stretching and rocking deformation [68]), 1206 and 1149 $cm^{-1}$ ($CF_2$ asymmetric and symmetric stretching vibration, respectively [69]) appeared also in the spectrum of T–PTFE–Fresh but with lower intensities. This decrease in the intensity of the peaks could be caused by the $TiO_2$ assembled on the surface of PTFE [70]. In the case of PVDF membranes containing mainly α–crystalline phase (Fig. S3d), the peaks corresponding to the asymmetrical and symmetrical stretching, and deformation vibration of $CH_2$ groups were exhibited at 3022 and 2990 $cm^{-1}$, and at 1395 $cm^{-1}$, respectively [71], while the peak attributed to $–CF_2$ groups was observed at 1177 $cm^{-1}$.

The surface hydrophilicity is a featured property for membranes used in pressure-driven processes and other water treatment systems. The hydrophilicity of neat and $TiO_2$ membranes was assessed by water contact angle measurements (Table 2 and Fig. 6). The neat PTFE and PVDF membranes can be considered moderately hydrophilic with contact angles in the range of 80–91º (Table 2), while N–PS was the most hydrophilic membrane with a contact angle of 56º. In general, $TiO_2$ membranes presented lower contact angles than their corresponding neat membranes (e.g., 80º and 76º for N–PVDF and T–PVDF, respectively). It is well-know that the addition or deposition of $TiO_2$ on/into a membrane enhances its surface hydrophilicity [72-75]. In our study, not only the addition of $TiO_2$ was important, but also the amount and the location where it was assembled on the membrane. Thus, large amounts of $TiO_2$ (i.e., 11.0 wt.%) forming particle clusters on the membrane markedly decreased the contact angle from 56° to 26° for PS membranes, while T– PTFE and T–PVDF with lower $TiO_2$ contents (i.e., 2.7 and 3.3 wt.%, respectively) assembled on the corresponding polymer structure presented a slightly lower hydrophilicity than their corresponding neat membranes (Fig. 6).

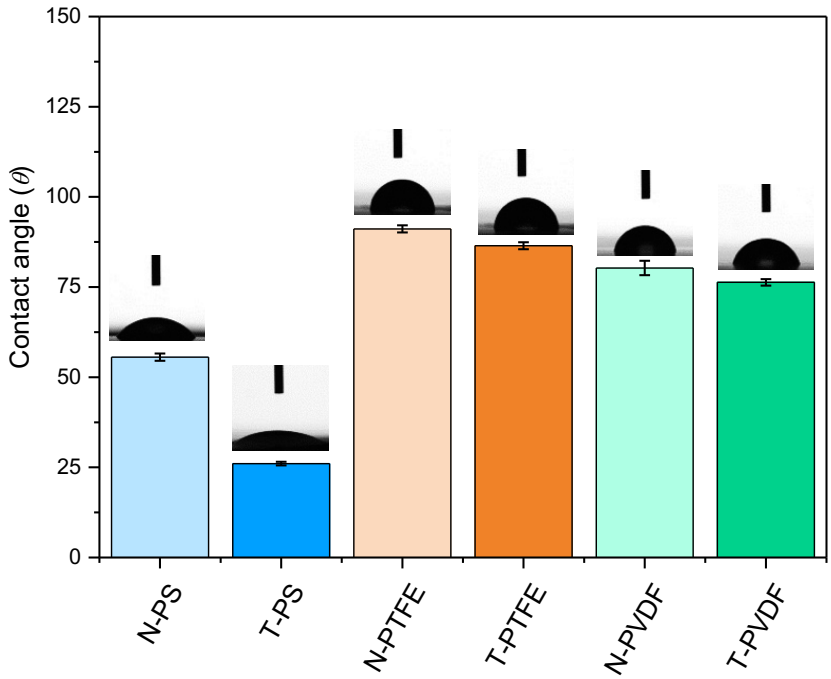


**Fig. 6.** Contact angle for the neat and $TiO_2$ membranes.

The binding of $TiO_2$ nanoparticles to the membrane is a crucial factor to hinder particle leaching and membrane fouling, which in turns would decrease of membrane performance during adsorption and photocatalytic experiments. Thus, the amount of $TiO_2$ leached from the membranes was determined during stability tests carried out in an ultrasonication bath for 30 min. In general, all $TiO_2$ membranes exhibited a good stability with a $TiO_2$ loss lower than 10 wt.% (Fig. 7) proving a strong attachment of $TiO_2$ nanoparticles to the membrane structure. The $TiO_2$ leached for 30 min varied as follows: T–PTFE (9.1 %) > T–PVDF (8.4 %) > T–PS (6.5 %), T–PS being the most stable membrane, even presenting the highest $TiO_2$ content. This enhanced binding of $TiO_2$ should be due to coordination bonds of the sulfone groups and ether bonds of the PS membrane and the hydroxyl groups of $TiO_2$ nanoparticles [53]. It is noteworthy than most of $TiO_2$ leached in both T–PVDF and T–PTFE was obtained in the first 2–5 min and then, it was maintained almost invariable. In the case of T-PSThe immobilization of $TiO_2$ nanoparticles in these hydrophilic membranes should be explained by coordination bonds between $Ti^{4+}$ of $TiO_2$ and the hydroxyl groups of the membranes [76], which were pre-

hydrophilized by the manufacturer with carboxyl groups [28]. In the case of T-PS, a sudden increase of the $TiO_2$ leached was observed after 10 min, which could be due to some changes in the membrane structure as a consequence of the applied ultrasounds and/or increased temperature of the bath. Otherwise, T-PS was the most stable membrane, the $TiO_2$ leaching being always lower than that obtained for T-PVDF and T-PTFE.

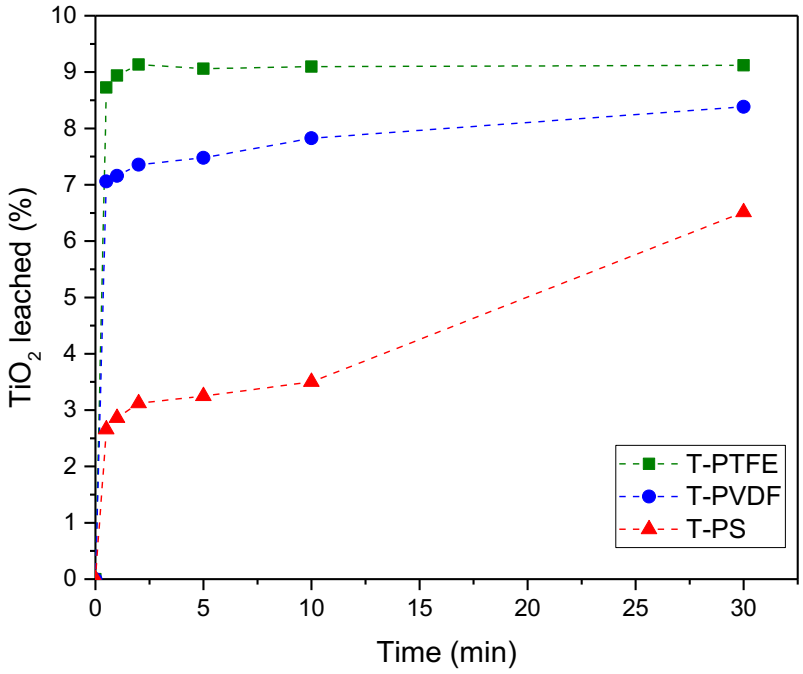


**Fig. 7.** Amount of $TiO_2$ leached for $TiO_2$ membranes during ultrasonication tests.

*3.2. Removal of diclofenac and 17α-ethinylestradiol under continuous recirculating mode*

3.2.1. Pollutants adsorption in dark phase

The capacity of adsorption or retention for neat and $TiO_2$ membranes was studied with an aqueous solution containing both DCF and EE2 pollutants, at room temperature, under continuous recirculating mode and for 24 h (Fig. 8). The dark phase was performed to saturate most of the membrane surface and consequently, to assess separately the photocatalytic activity of $TiO_2$ membranes. Considering that the molecular size of the studied pollutant molecules (0.414 nm [77] and 1.53 nm [78] for DCF and EE2, respectively) is much smaller than the nominal pore size of the PS, PTFE and PVDF membranes (nearly 0.2 µm, Table 1), the removal

of the pollutants in the dark should be more likely due to the adsorption ability of the membranes rather than physical retention of these pollutants.

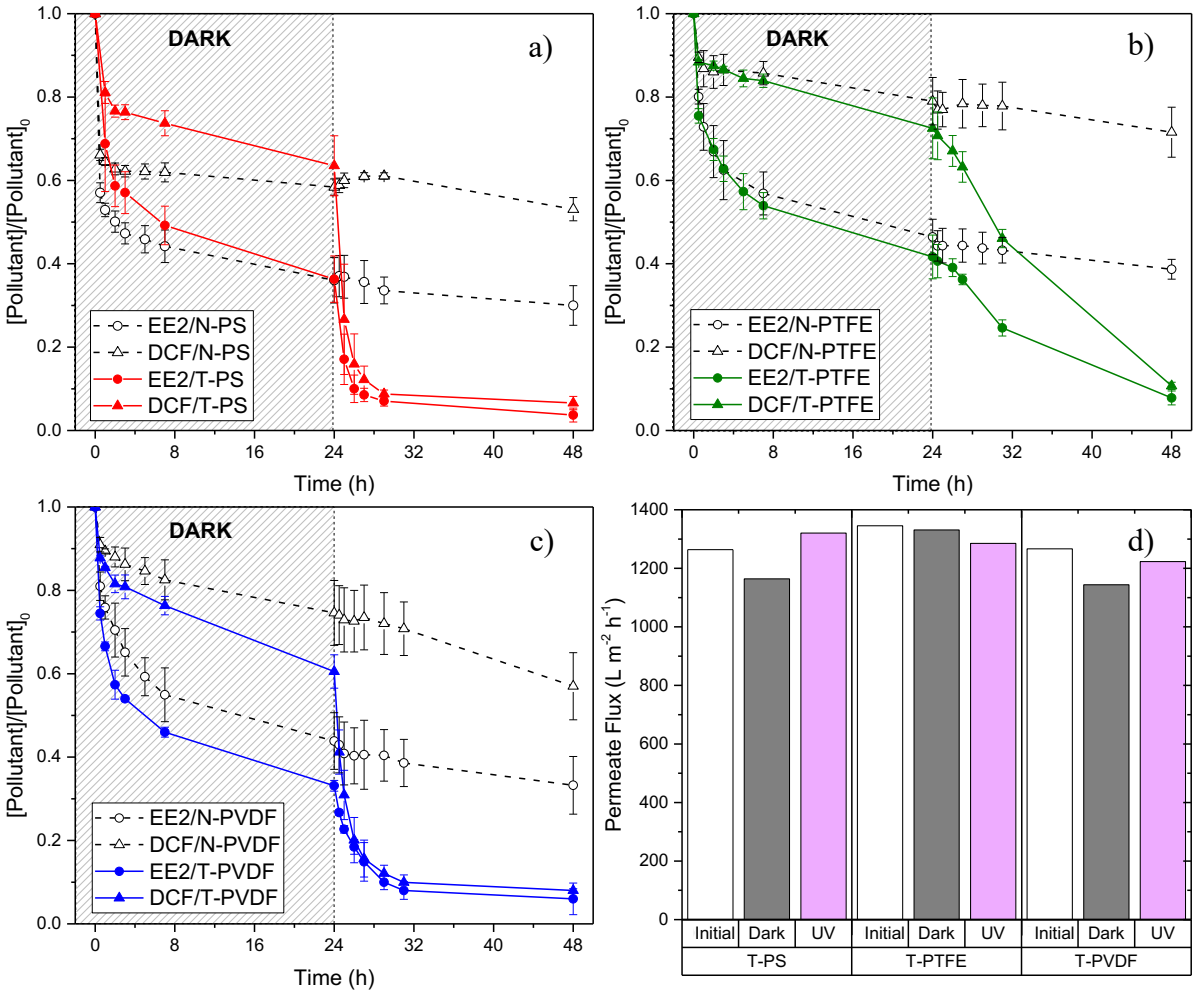


**Fig. 8.** Normalized pollutant concentration for adsorption and photodegradation of DCF and EE2 using (a) N–PS and T–PS, (b) N–PTFE and T–PTFE, and (c) N–PVDF and T–PVDF. (d) Permeate flux of the $TiO_2$ membranes measured initially (at 0.5 h), under dark conditions (at 24 h) and UV-LED irradiation (at 48 h).

In general, $TiO_2$ membranes prepared with PVDF and PTFE supports exhibited higher removals (%) by adsorption for DCF (39 and 25 % for T–PVDF and N–PVDF, respectively) and EE2 (67 and 56 %, respectively) than their corresponding neat membranes (Figs. 8b-c), which could be attributed to the enhanced hydrophilicity of these membranes after immobilizing $TiO_2$

nanoparticles on their structures, favouring the contact between pollutant molecules in aqueous solution and the membranes surface. Moreover, T–PVDF with a lower water contact angle (Table 2) presented higher removals by adsorption than T–PTFE. On contrast, the pollutants adsorption over N–PS was higher than that obtained for T–PS (Figs. 8a) and although the $TiO_2$ deposition enhanced its hydrophilicity, the significant decrease in porosity detected for T–PS (from 71 % to 35 %, Table 2) affected considerably the adsorptive behaviour.

On the other hand, the removal by adsorption of the EE2 contaminant was always higher than that of DCF regardless of the type of membrane tested (Figs. 8a-c). This competitive adsorption is explained by the interactions established between the pollutant molecules and the membrane surface. Taking into account that the p*K*a values of EE2 and DCF are 10.3 [45] and 4.2 [39], respectively, and the pH in experiments with ultrapure water was ca. 6.5, EE2 molecules are mostly neutral while DCF ones are negatively charged. Furthermore, the pH of the point zero charge ($pH_{PZC}$) for $TiO_2$ membranes could be considered close to the bare $TiO_2$ material ($pH_{PZC}$ ≈ 6.0 [31, 79]) and thereby, all $TiO_2$ membranes are expected to present a negatively charged surface at the conditions of the experiments, explaining the preferential adsorption of EE2 instead of DCF (electrostatic repulsions). Besides, DCF is a pharmaceutical slightly more hydrophobic than EE2, i.e., log $K_{ow}$ = 4.51 [39] and 3.63 [45] for DFC and EE2, respectively, which would also explain the lower DCF adsorption detected in the hydrophilic $TiO_2$ membranes.

#### 3.2.2. Removal efficiency of DCF/EE2 at 24 h (Dark) and 48 h (UV) for all membranes. Photocatalytic degradation of DCF and EE2

The efficiency of the neat and $TiO_2$ membranes for the simultaneous photodegradation of DCF and EE2 in aqueous solution under UV–LED irradiation is also shown in Fig. 8. All membranes were almost saturated during the dark phase at 24 h, although a slight increase in the removal of both pollutants is still detected for neat membranes after turning on UV–LED (Fig. 8). All

$TiO_2$ membranes were able to photodegrade DCF and EE2 with efficiencies above 90 % after 24 h of UV–LED irradiation (e.g., 96, 94 and 92 % for EE2 using T–PS, T–PVDF and T–PTFE, respectively), as clearly shown in Fig. 8a for T–PS, where the evolution of the pollutants concentration dropped quickly after turning on the UV–LED irradiation. On contrast, these curves for neat membranes followed the same profile than those obtained during the dark phase (Figs. 8a-c), indicating the absence of photolysis of the tested pollutants at 395 nm, and that the decrease in the concentration of DCF and EE2 was due to the adsorption ability of the membranes, which allows the pollutants accumulation on the membrane surface and is favoured by a large overall porosity and/or hydrophilicity.

Among the developed $TiO_2$ membranes, T–PS was the most active for the removal of DCF (93 %) and EE2 (96 %), followed by T–PVDF (92 % and 94 % for DCF and EE2, respectively) and finally T–PTFE (89 % and 92 % for DCF and EE2, respectively), for 24 h under UV–LED irradiation (Fig. 8a-c). As pointed out, the EE2 removal was always higher than that for DCF regardless of the type of the membrane, and the activity trend seems be directly correlated with the $TiO_2$ content attached in the membranes, since T–PS possessed the highest content (11.0 wt.%, Table 2). It is noteworthy that T–PTFE was much less photoactive than the other $TiO_2$ membranes during short reaction times (i.e., 0.5 – 3 h), although its $TiO_2$ content is similar to that of T–PVDF, which exhibited a reaction kinetic similar to T–PS. This fact could be explained by the difference in wettability among $TiO_2$ membranes, T–PTFE being the least hydrophilic. Thus, photoactivity of T-PS was similar to that of T-PVDF despite the large difference in the $TiO_2$ content between these two membranes (11.0 and 3.3 wt.%, respectively, cf. Table 2), suggesting that the photoactivity is also related to the way as the catalyst is deposited on the membrane, where the self-assembling of $TiO_2$ in the form of clusters on the surface of the PS membrane could reduce the number of $TiO_2$ particles accessible to UV-LED irradiation.

Finally, the permeate flux of all membranes was measured initially and after dark and UV-LED irradiation stages, as shown in Fig. 8d for $TiO_2$ membranes. The permeate fluxes for neat membranes (results not shown) were higher than those measured for the corresponding $TiO_2$ membranes, which was attributed to the pore blockage occurring in membrane supports after the $TiO_2$ deposition. For instance, the initial water flux varied from 1413 to 1264 LMH for N–PS and T–PS respectively. As described in Section 3.2.1, DCF and EE2 pollutants were adsorbed on the membrane surface during the dark phase, this contaminant accumulation affecting on the membrane permeability. Thus, a decrease of the permeate flux at 24 h was always obtained for all membranes tested, this permeability lost being correlated with the amount of adsorbed contaminants, since T–PTFE was the least affected (Fig. 8d), i.e., 1331 LMH for T–PTFE in comparison with 1164 and 1144 LMH for T–PS and T–PVDF, respectively. Otherwise, the fluxes of $TiO_2$ membranes were high enough to be employed in UV–LED photocatalysis under continuous recirculating mode. Thus, by switching on the UV–LED, the permeate fluxes with the T–PS and T–PVDF membranes increased (Fig. 8d), suggesting the photocatalytic degradation of contaminant molecules adsorbed on the membrane surface due to the activity of the photocatalyst deposited on the membrane [31]. This enhancement of the water permeability could also be attributed to the high hydrophilicity of $TiO_2$ membranes resulting from the strong interaction of the $TiO_2$ particles with water molecules under UV irradiation [74, 80]. In addition, the increase of water permeate flux in T–PS and T–PVDF was higher than that recorded for T–PTFE, which could be correlated with the photoactivity of the membranes, since T–PS and T–PVDF were more photocatalytic active (Fig. 8a-c). On the other hand, the permeate flux for T–PTFE and T–PVDF at 48 h was slightly lower than that determined initially (at 0.5 h), which it increased for T–PS. Most probably, the continuous increase in the flux for T-PS was related to the deterioration of the membrane structure and its fracture (as shown below in Fig. 9c), due to the low resistance of polysulfone

polymer against UV irradiation and hydroxyl radicals generated during the photocatalytic reaction [35].

### 3.2.3. Membrane stability during consecutive reaction cycles

The efficiency and stability of $TiO_2$ membranes were investigated for the simultaneous removal of DCF and EE2 during three consecutive adsorption-photocatalysis cycles, maintaining the same membrane and without applying any cleaning or regeneration step (Figs. 9a-b). As concluded, T–PS was the most active membrane but it was excluded from this study because it was damaged after first adsorption-photocatalysis cycle (Fig. 9c), as a consequence of the $TiO_2$ leaching for 48 h and the low resistance of the polysulfone polymer to UV exposure and hydroxyl radicals generated during reaction [35]. In fact, the permeate flux measured for this membrane after UV–LED irradiation was higher than that initially determined for the fresh membrane (Fig. 8d), corroborating possible particle leaching and possible damages in the membrane structure. On the other hand, both T–PTFE and T–PVDF were stable during all the reaction cycles, without any appreciable damages on their structures, as corroborated by comparing fresh and spent membranes (Fig. 9c). Both membranes were active in the consecutive reaction cycles for the removal of DCF and EE2. However, a significant decrease of the membrane performance was detected after first cycle, particularly for T–PTFE (Fig. 9a *vs.* 9b and Table 3), which may be ascribed to the pollutant adsorption on the membrane surface [30, 31] and partial $TiO_2$ leaching. These photocatalytic results can be correlated with the permeate flux measured at the end of each irradiation cycle, where an increased flux was detected after the first cycle of irradiation (Fig. 9d). On the contrary, T–PVDF presented the highest activity for removing both DCF and EE2 and excellent stability under UV–LED irradiation for 4 days (Figs. 9b-d and Table 3). In addition, the permeate flux at 96 h was comparable to the initial one, suggesting that all contaminant adsorbed on the membrane surface can be degraded by UV–LED exposure. Overall, the $TiO_2$ membrane prepared on the PVDF

membrane resulted as a good option for treating water polluted with pharmaceuticals during long operation times. Thus, this PMR with the photocatalyst immobilized onto PVDF membranes has the advantage to mitigate the fouling, to achieve high fluxes, to be reasonable stable and highly active for the simultaneous degradation of water pollutants under UV-LED and continuous recirculating mode, being easily scaled up since it does not require the recovery and regeneration of the catalyst, which would be time and energy-consuming and costly.

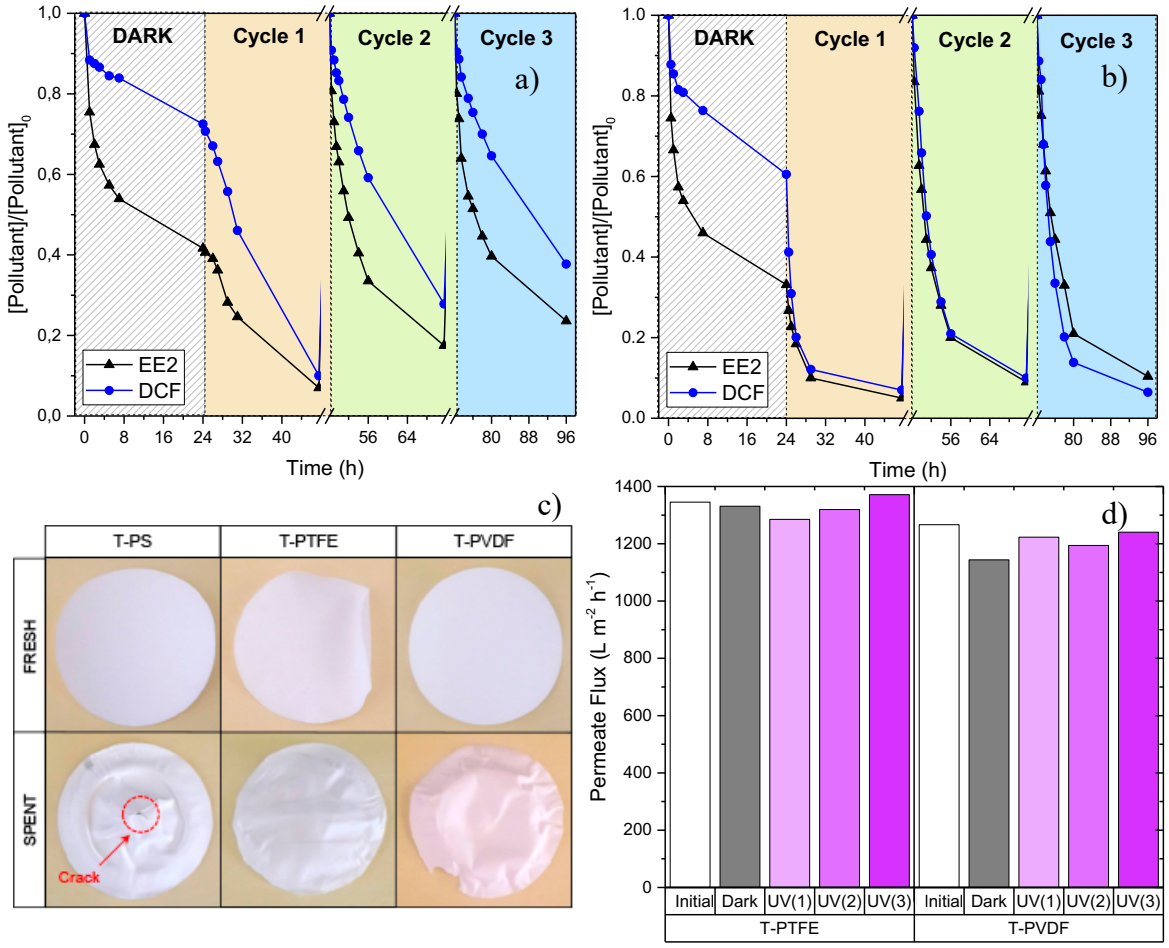


**Fig. 9.** Membrane performance during three consecutive reaction cycles for (a) T–PTFE and (b) T–PVDF. (c) Images of the fresh and spent $TiO_2$ membranes. (d) Permeate flux of T–PTFE and T–PVDF measured initially (at 0.5 h), under dark conditions (at 24 h) and after all UV–LED cycles (at 48, 72 and 96 h).

## 4. Conclusions

$TiO_2$ membranes were prepared by *in situ* growth of $TiO_2$ over PS, PTFE and PVDF supports. The content of $TiO_2$ in these membranes is affected by the corresponding structure and surface hydrophilicity of the support. The highest amount of $TiO_2$ was achieved on the PS surface, but a significant decrease in the porosity was also observed.

Anatase $TiO_2$ crystalline phase was formed on these supports by hydrothermal treatment at mild conditions, which allowed the preservation of the original structure of the polymeric support and increased the surface hydrophilicity. Neat and $TiO_2$ membranes were then studied for the simultaneous removal of DCF and EE2 in an aqueous solution under adsorption and photocatalytic experiments.

Neat membranes could not wholly remove the pollutants, but a higher porosity and hydrophilicity favoured their adsorptive behaviour. EE2 was preferentially removed over DCF regardless of the membrane tested due to the electrostatic repulsions between the DCF molecules and the surface of these membranes.

All $TiO_2$ membranes achieved efficiencies above 90 % for both pollutants under UV–LED irradiation; their performance is improved as the $TiO_2$ content and the hydrophilicity increased. The permeate flux of both neat and $TiO_2$ membranes decreased under dark conditions, suggesting that the contaminants are adsorbed and accumulated on the membrane surface. However, the permeate flux enhanced when $TiO_2$ membranes were exposed to UV-LED irradiation. From the stability assays during several consecutive reaction cycles, it was concluded that the $TiO_2$ membrane with PVDF presents the highest stability.

## Acknowledgements

This work was financially supported by project POCI-01-0145-FEDER-029600 (2DMAT4FUEL) funded by FEDER through COMPETE2020 – POCI and with

financial support from FCT/MCTES, through national funds (PIDDAC). We would also like to thank the scientific collaboration under project Base Funding – UIDB/50020/2020 of the Associate Laboratory LSRE-LCM – funded by national funds through FCT/MCTES (PIDDAC), the Spanish Projects ref. RTI2018-099224-B-I00 and PID2019-107033GB-C22 from ERDF/Ministry of Science, Innovation and Universities – State Research Agency, and the Nano4Fresh project (ref. PCI2020-112045), as part of the PRIMA Programme supported by the European Union. SD acknowledges the Erasmus Mundus Programme. SMT acknowledges the Spanish Ministry of Economy and Competitiveness (MINECO), the State Research Agency and the European Social Found for a Ramón y Cajal research contract (RYC-2019-026634-I/AEI/10.13039/501100011033). ARR acknowledges FCT funding under DL57/2016 Transitory Norm Programme. Dr. Carlos Sá and CEMUP team (Portugal) are gratefully acknowledged for the technical assistance with SEM analysis.

**References**

[1] T. Deblonde, C. Cossu-Leguille, P. Hartemann, Emerging pollutants in wastewater: a review of the literature, Int. J. Hyg. Environ. Health, 214 (2011) 442-448.

[2] J. Hofmann, U. Freier, M. Wecks, S. Hohmann, Degradation of diclofenac in water by heterogeneous catalytic oxidation with $H_2O_2$, Appl. Catal. B-Environ., 70 (2007) 447-451.

[3] P. Verlicchi, M. Al Aukidy, A. Galletti, M. Petrovic, D. Barcelo, Hospital effluent: investigation of the concentrations and distribution of pharmaceuticals and environmental risk assessment, Sci. Total Environ., 430 (2012) 109-118.

[4] Y. Luo, W. Guo, H.H. Ngo, L.D. Nghiem, F.I. Hai, J. Zhang, S. Liang, X.C. Wang, A review on the occurrence of micropollutants in the aquatic environment and their fate and removal during wastewater treatment, Sci. Total Environ., 473-474 (2014) 619-641.

[5] E.N. Evgenidou, I.K. Konstantinou, D.A. Lambropoulou, Occurrence and removal of transformation products of PPCPs and illicit drugs in wastewaters: a review, Sci. Total Environ., 505 (2015) 905-926.

[6] R. Vinoth Kumar, M.O. Barbosa, A.R. Ribeiro, S. Morales-Torres, M.F.R. Pereira, A.M.T. Silva, Advanced oxidation technologies combined with direct contact membrane distillation for treatment of secondary municipal wastewater, Process Saf. Environ. Prot., 140 (2020) 111-123.

[7] Commission implementing decision (EU) 2020/1161 of 4 August 2020 establishing a watch list of substances for Union-wide monitoring in the field of water policy pursuant to directive 2008/105/EC of the European parliament and of the council, Off. J. Eur. Union, 257 L (2020) 32-35.

[8] B. Czech, W. Buda, Multicomponent nanocomposites for elimination of diclofenac in water based on an amorphous $TiO_2$ active in various light sources, J. Photochem. Photobiol., A, 330 (2016) 64-70.

[9] A. Mavragani, K. Sypsa, A. Sampri, K.P. Tsagarakis, Quantifying the UK Online Interest in Substances of the EU Watchlist for Water Monitoring: Diclofenac, Estradiol, and the Macrolide Antibiotics, Water-Sui, 8 (2016) 542.

[10] P. Schroder, B. Helmreich, B. Skrbic, M. Carballa, M. Papa, C. Pastore, Z. Emre, A. Oehmen, A. Langenhoff, M. Molinos, J. Dvarioniene, C. Huber, K.P. Tsagarakis, E. Martinez-Lopez, S.M. Pagano, C. Vogelsang, G. Mascolo, Status of hormones and painkillers in wastewater effluents across several European states-considerations for the EU watch list concerning estradiols and diclofenac, Environ. Sci. Pollut. Res., 23 (2016) 12835-12866.

[11] S. Zorita, L. Martensson, L. Mathiasson, Occurrence and removal of pharmaceuticals in a municipal sewage treatment system in the south of Sweden, Sci. Total Environ., 407 (2009) 2760-2770.

[12] Y. Zuo, K. Zhang, S. Zhou, Determination of estrogenic steroids and microbial and photochemical degradation of 17alpha-ethinylestradiol (EE2) in lake surface water, a case study, Environ. Sci.: Process. Impacts, 15 (2013) 1529-1535.

[13] A.Z. Aris, A.S. Shamsuddin, S.M. Praveena, Occurrence of 17alpha-ethynylestradiol (EE2) in the environment and effect on exposed biota: a review, Environ. Int., 69 (2014) 104-119.

[14] M. Sillanpaa, M.C. Ncibi, A. Matilainen, Advanced oxidation processes for the removal of natural organic matter from drinking water sources: A comprehensive review, J. Environ. Manage., 208 (2018) 56-76.

[15] M.I.G. Miranda, C.I.D. Bica, S.M.B. Nachtigall, N. Rehman, S.M.L. Rosa, Kinetical thermal degradation study of maize straw and soybean hull celluloses by simultaneous DSC-TGA and MDSC techniques, Thermochim. Acta, 565 (2013) 65-71.

[16] P. Calza, V.A. Sakkas, C. Medana, C. Baiocchi, A. Dimou, E. Pelizzetti, T. Albanis, Photocatalytic degradation study of diclofenac over aqueous $TiO_2$ suspensions, Appl. Catal. B-Environ., 67 (2006) 197-205.

[17] M. Pelaez, N.T. Nolan, S.C. Pillai, M.K. Seery, P. Falaras, A.G. Kontos, P.S.M. Dunlop, J.W.J. Hamilton, J.A. Byrne, K. O'Shea, M.H. Entezari, D.D. Dionysiou, A review on the visible light active titanium dioxide photocatalysts for environmental applications, Appl. Catal. B-Environ., 125 (2012) 331-349.

[18] S. Morales-Torres, L.M. Pastrana-Martinez, J.L. Figueiredo, J.L. Faria, A.M. Silva, Design of graphene-based $TiO_2$ photocatalysts--a review, Environ. Sci. Pollut. Res., 19 (2012) 3676-3687.

[19] J.F. García-Araya, F.J. Beltrán, A. Aguinaco, Diclofenac removal from water by ozone and photolytic $TiO_2$ catalysed processes, J. Chem. Technol. Biotechnol., 85 (2010) 798-804.

[20] J. Schneider, M. Matsuoka, M. Takeuchi, J. Zhang, Y. Horiuchi, M. Anpo, D.W. Bahnemann, Understanding $TiO_2$ photocatalysis: mechanisms and materials, Chem. Rev., 114 (2014) 9919-9986.

[21] F. Mendez-Arriaga, S. Esplugas, J. Gimenez, Photocatalytic degradation of non-steroidal anti-inflammatory drugs with $TiO_2$ and simulated solar irradiation, Water Res., 42 (2008) 585-594.

[22] A. Achilleos, E. Hapeshi, N.P. Xekoukoulotakis, D. Mantzavinos, D. Fatta-Kassinos, Factors affecting diclofenac decomposition in water by UV-A/$TiO_2$ photocatalysis, Chem. Eng. J., 161 (2010) 53-59.

[23] D. Kanakaraju, B.D. Glass, M. Oelgemöller, Titanium dioxide photocatalysis for pharmaceutical wastewater treatment, Environ. Chem. Lett., 12 (2013) 27-47.

[24] S. Mozia, Photocatalytic membrane reactors (PMRs) in water and wastewater treatment. A review, Sep. Purif. Technol., 73 (2010) 71-91.

[25] B.L. Phoon, C.C. Ong, M.S. Mohamed Saheed, P.-L. Show, J.-S. Chang, T.C. Ling, S.S. Lam, J.C. Juan, Conventional and emerging technologies for removal of antibiotics from wastewater, J. Hazard. Mater., 400 (2020) 122961.

[26] E. Bet-moushoul, Y. Mansourpanah, K. Farhadi, M. Tabatabaei, $TiO_2$ nanocomposite based polymeric membranes: A review on performance improvement for various applications in chemical engineering processes, Chem. Eng. J., 283 (2016) 29-46.

[27] Q. Wang, C. Yang, G. Zhang, L. Hu, P. Wang, Photocatalytic Fe-doped $TiO_2$/PSF composite UF membranes: Characterization and performance on BPA removal under visible-light irradiation, Chem. Eng. J., 319 (2017) 39-47.

[28] K. Fischer, M. Grimm, J. Meyers, C. Dietrich, R. Glaser, A. Schulze, Photoactive microfiltration membranes via directed synthesis of $TiO_2$ nanoparticles on the polymer surface for removal of drugs from water, J. Membr. Sci., 478 (2015) 49-57.

[29] K. Fischer, P. Schulz, I. Atanasov, A.A. Latif, I. Thomas, M. Kuhnert, A. Prager, J. Griebel, A. Schulze, Synthesis of High Crystalline $TiO_2$ Nanoparticles on a Polymer Membrane to Degrade Pollutants from Water, Catalysts, 8 (2018) 376.

[30] C.P. Athanasekou, S. Morales-Torres, V. Likodimos, G.E. Romanos, L.M. Pastrana-Martinez, P. Falaras, D.D. Dionysiou, J.L. Faria, J.L. Figueiredo, A.M.T. Silva, Prototype composite membranes of partially reduced graphene oxide/$TiO_2$ for photocatalytic ultrafiltration water treatment under visible light, Appl. Catal. B-Environ., 158 (2014) 361-372.

[31] L.M. Pastrana-Martinez, S. Morales-Torres, J.L. Figueiredo, J.L. Faria, A.M.T. Silva, Graphene oxide based ultrafiltration membranes for photocatalytic degradation of organic pollutants in salty water, Water Res., 77 (2015) 179-190.

[32] L.M. Pastrana-Martínez, S. Morales-Torres, S.K. Papageorgiou, F.K. Katsaros, G.E. Romanos, J.L. Figueiredo, J.L. Faria, P. Falaras, A.M.T. Silva, Photocatalytic behaviour of nanocarbon–$TiO_2$ composites and immobilization into hollow fibres, Appl. Catal. B-Environ., 142-143 (2013) 101-111.

[33] Y. Shi, J. Huang, G. Zeng, W. Cheng, J. Hu, Photocatalytic membrane in water purification: is it stepping closer to be driven by visible light?, J. Membr. Sci., 584 (2019) 364-392.

[34] Z.A.M. Hir, P. Moradihamedani, A.H. Abdullah, M.A. Mohamed, Immobilization of $TiO_2$ into polyethersulfone matrix as hybrid film photocatalyst for effective degradation of methyl orange dye, Mater. Sci. Semicond. Process., 57 (2017) 157-165.

[35] S.S. Chin, K. Chiang, A.G. Fane, The stability of polymeric membranes in a $TiO_2$ photocatalysis process, J. Membr. Sci., 275 (2006) 202-211.

[36] L. Paredes, S. Murgolo, H. Dzinun, M.H.D. Othman, A.F. Ismail, M. Carballa, G. Mascolo, Application of immobilized $TiO_2$ on PVDF dual layer hollow fibre membrane to improve the

photocatalytic removal of pharmaceuticals in different water matrices, Appl. Catal. B-Environ., 240 (2019) 9-18.

[37] H.C. Song, J.H. Shao, Y.L. He, B. Liu, X.Q. Zhong, Natural organic matter removal and flux decline with PEG-$TiO_2$-doped PVDF membranes by integration of ultrafiltration with photocatalysis, J. Membr. Sci., 405 (2012) 48-56.

[38] N.K.O. Cruz, G.U. Semblante, D.B. Senoro, S.J. You, S.C. Lu, Dye degradation and antifouling properties of polyvinylidene fluoride/titanium oxide membrane prepared by sol-gel method, J. Taiwan Inst. Chem. Eng., 45 (2014) 192-201.

[39] K.V. Plakas, V.C. Sarasidis, S.I. Patsios, D.A. Lambropoulou, A.J. Karabelas, Novel pilot scale continuous photocatalytic membrane reactor for removal of organic micropollutants from water, Chem. Eng. J., 304 (2016) 335-343.

[40] D. Darowna, S. Grondzewska, A.W. Morawski, S. Mozia, Removal of non-steroidal anti-inflammatory drugs from primary and secondary effluents in a photocatalytic membrane reactor, J. Chem. Technol. Biotechnol., 89 (2014) 1265-1273.

[41] F. Martinez, M.J. Lopez-Munoz, J. Aguado, J.A. Melero, J. Arsuaga, A. Sotto, R. Molina, Y. Segura, M.I. Pariente, A. Revilla, L. Cerro, G. Carenas, Coupling membrane separation and photocatalytic oxidation processes for the degradation of pharmaceutical pollutants, Water Res., 47 (2013) 5647-5658.

[42] V.C. Sarasidis, K.V. Plakas, S.I. Patsios, A.J. Karabelas, Investigation of diclofenac degradation in a continuous photo-catalytic membrane reactor. Influence of operating parameters, Chem. Eng. J., 239 (2014) 299-311.

[43] R.M. Castellanos, J.P. Bassin, M. Dezotti, R.A.R. Boaventura, V.J.P. Vilar, Tube-in-tube membrane reactor for heterogeneous $TiO_2$ photocatalysis with radial addition of $H_2O_2$, Chem. Eng. J., 395 (2020) 124998.

[44] B.K. Mayer, C. Johnson, Y. Yang, N. Wellenstein, E. Maher, P.J. McNamara, From micro to macro-contaminants: The impact of low-energy titanium dioxide photocatalysis followed by filtration on the mitigation of drinking water organics, Chemosphere, 217 (2019) 111-121.

[45] M.J. Arlos, R. Liang, M.M. Hatat-Fraile, L.M. Bragg, N.Y. Zhou, M.R. Servos, S.A. Andrews, Photocatalytic decomposition of selected estrogens and their estrogenic activity by UV-LED irradiated $TiO_2$ immobilized on porous titanium sheets via thermal-chemical oxidation, J. Hazard. Mater., 318 (2016) 541-550.

[46] L.M. Pastrana-Martínez, S. Morales-Torres, V. Likodimos, J.L. Figueiredo, J.L. Faria, P. Falaras, A.M.T. Silva, Advanced nanostructured photocatalysts based on reduced graphene oxide–$TiO_2$ composites for degradation of diphenhydramine pharmaceutical and methyl orange dye, Appl. Catal. B-Environ., 123-124 (2012) 241-256.

[47] S. Brunauer, P.H. Emmett, E. Teller, Adsorption of gases in multimolecular layers, J. Am. Chem. Soc., 60 (1938) 309-319.

[48] F. Rouquerol, J. Rouquerol, K.S.W. Sing, Adsorption by Powders and Porous Solids. Principles, Methodology and Applications, Academic Press, London, 1999.

[49] T.L.S. Silva, S. Morales-Torres, J.L. Figueiredo, A.M.T. Silva, Multi-walled carbon nanotube/PVDF blended membranes with sponge- and finger-like pores for direct contact membrane distillation, Desalination, 357 (2015) 233-245.

[50] S. Morales-Torres, C.M.P. Esteves, J.L. Figueiredo, A.M.T. Silva, Thin-film composite forward osmosis membranes based on polysulfone supports blended with nanostructured carbon materials, Journal of Membrane Science, 520 (2016) 326-336.

[51] J. Stötzel, D. Lützenkirchen-Hecht, R. Frahm, C.V. Santilli, S.H. Pulcinelli, R. Kaminski, E. Fonda, F. Villain, V. Briois, QEXAFS and UV/Vis Simultaneous Monitoring of the $TiO_2$-Nanoparticles Formation by Hydrolytic Sol-Gel Route, J. Phys. Chem. C 114 (2010) 6228–6236.

[52] N.F.F. Moreira, C.A. Orge, A.R. Ribeiro, J.L. Faria, O.C. Nunes, M.F.R. Pereira, A.M.T. Silva, Fast mineralization and detoxification of amoxicillin and diclofenac by photocatalytic ozonation and application to an urban wastewater, Water Res., 87 (2015) 87-96.

[53] M.L. Luo, J.Q. Zhao, W. Tang, C.S. Pu, Hydrophilic modification of poly(ether sulfone) ultrafiltration membrane surface by self-assembly of $TiO_2$ nanoparticles, Appl. Surf. Sci., 249 (2005) 76-84.

[54] M. Kemell, E. Farm, M. Ritala, M. Leskela, Surface modification of thermoplastics by atomic layer deposition of $Al_2O_3$ and $TiO_2$ thin films, Eur. Polym. J., 44 (2008) 3564-3570.

[55] O. Iglesias, M.J. Rivero, A.M. Urtiaga, I. Ortiz, Membrane-based photocatalytic systems for process intensification, Chem. Eng. J., 305 (2016) 136-148.

[56] W. Krengvirat, S. Sreekantan, A.F.M. Noor, N. Negishi, G. Kawamura, H. Muto, A. Matsuda, Low-temperature crystallization of $TiO_2$ nanotube arrays via hot water treatment and their photocatalytic properties under visible-light irradiation, Mater. Chem. Phys., 137 (2013) 991-998.

[57] M.A. Henderson, A surface science perspective on $TiO_2$ photocatalysis, Surf. Sci. Rep., 66 (2011) 185-297.

[58] Y. Qian, L. Chi, W. Zhou, Z. Yu, Z. Zhang, Z. Zhang, Z. Jiang, Fabrication of $TiO_2$-modified polytetrafluoroethylene ultrafiltration membranes via plasma-enhanced surface graft pretreatment, Appl. Surf. Sci., 360 (2016) 749-757.

[59] M.M. Ba-Abbad, A.A.H. Kadhum, A.B. Mohamad, M.S. Takriff, Synthesis and Catalytic Activity of $TiO_2$ Nanoparticles for Photochemical Oxidation of Concentrated Chlorophenols under Direct Solar Radiation, Int. J. Electrochem. Sci., 7 (2012) 4871 - 4888.

[60] M. Safarpour, A. Khataee, V. Vatanpour, Preparation of a Novel Polyvinylidene Fluoride (PVDF) Ultrafiltration Membrane Modified with Reduced Graphene Oxide/Titanium Dioxide

(TiO2) Nanocomposite with Enhanced Hydrophilicity and Antifouling Properties, Ind. Eng. Chem. Res., 53 (2014) 13370-13382.

[61] M. Safarpour, A. Khataee, V. Vatanpour, Effect of reduced graphene oxide/$TiO_2$ nanocomposite with different molar ratios on the performance of PVDF ultrafiltration membranes, Sep. Purif. Technol., 140 (2015) 32-42.

[62] U.N. Rusli, N.H. Alias, M.Z. Shahruddin, N.H. Othman, Photocatalytic Degradation of Oil using Polyvinylidene Fluoride/Titanium Dioxide Composite Membrane for Oily Wastewater Treatment, MATEC Web Conf., 69 (2016) 05003.

[63] S.J. You, G.U. Semblante, S.C. Lu, R.A. Damodar, T.C. Wei, Evaluation of the antifouling and photocatalytic properties of poly(vinylidene fluoride) plasma-grafted poly(acrylic acid) membrane with self-assembled $TiO_2$, J Hazard Mater, 237-238 (2012) 10-19.

[64] F. Liu, M.R.M. Abed, K. Li, Preparation and characterization of poly(vinylidene fluoride) (PVDF) based ultrafiltration membranes using nano γ-$Al_2O_3$, J. Membr. Sci., 366 (2011) 97-103.

[65] M.A. Mohamed, J. Jaafar, A.F. Ismail, M.H.D. Othman, M.A. Rahman, Fourier Transform Infrared (FTIR) Spectroscopy, Membrane Characterization2017, pp. 3-29.

[66] K. Singh, S. Devi, H.C. Bajaj, P. Ingole, J. Choudhari, H. Bhrambhatt, Optical Resolution of Racemic Mixtures of Amino Acids through Nanofiltration Membrane Process, Sep. Sci. Technol., 49 (2014) 2630-2641.

[67] A.K. Nair, P.M. Shalin, P.E. JagadeeshBabu, Performance enhancement of polysulfone ultrafiltration membrane using $TiO_2$ nanofibers, Desalin. Water Treat., 57 (2015) 10506-10514.

[68] V. Satulu, B. Mitu, V.A. Altynov, N.E. Lizunov, L. Kravets, G. Dinescu, Synthesis and characterization of porous composite membranes with hydrophilic/hydrophobic sides, Thin Solid Films, 630 (2017) 92-99.

[69] J. Qiu, J. Ni, M. Zhai, J. Peng, H. Zhou, J. Li, G. Wei, Radiation grafting of styrene and maleic anhydride onto PTFE membranes and sequent sulfonation for applications of vanadium redox battery, Radiat. Phys. Chem., 76 (2007) 1703-1707.

[70] Q. Wang, X. Wang, Z. Wang, J. Huang, Y. Wang, PVDF membranes with simultaneously enhanced permeability and selectivity by breaking the tradeoff effect via atomic layer deposition of TiO2, J. Membr. Sci., 442 (2013) 57-64.

[71] F. Shi, Y. Ma, J. Ma, P. Wang, W. Sun, Preparation and characterization of PVDF/$TiO_2$ hybrid membranes with different dosage of nano-$TiO_2$, J. Membr. Sci., 389 (2012) 522-531.

[72] R.A. Damodar, S.J. You, H.H. Chou, Study the self cleaning, antibacterial and photocatalytic properties of $TiO_2$ entrapped PVDF membranes, J. Hazard. Mater., 172 (2009) 1321-1328.

[73] L.N. Chi, Y.J. Qian, B.Y. Zhang, Z.J. Zhang, Z. Jiang, Surface engineering and self-cleaning properties of the novel $TiO_2$/PAA/PTFE ultrafiltration membranes, Appl. Petrochem. Res., 6 (2016) 225-233.

[74] Y. Gao, M. Hu, B.X. Mi, Membrane surface modification with $TiO_2$-graphene oxide for enhanced photocatalytic performance, J. Membr. Sci., 455 (2014) 349-356.

[75] S.B. Teli, S. Molina, A. Sotto, E. Garcia-Calvo, J. de Abajo, Fouling Resistant Polysulfone-PANI/$TiO_2$ Ultrafiltration Nanocomposite Membranes, Ind. Eng. Chem. Res., 52 (2013) 9470-9479.

[76] L. Shao, Z.X. Wang, Y.L. Zhang, Z.X. Jiang, Y.Y. Liu, A facile strategy to enhance PVDF ultrafiltration membrane performance via self-polymerized polydopamine followed by hydrolysis of ammonium fluotitanate, J. Membr. Sci., 461 (2014) 10-21.

[77] K.V. Plakas, A. Mantza, S.D. Sklari, V.T. Zaspalis, A.J. Karabelas, Heterogeneous Fenton-like oxidation of pharmaceutical diclofenac by a catalytic iron-oxide ceramic microfiltration membrane, Chem. Eng. J., 373 (2019) 700-708.

[78] J. Han, S. Meng, Y. Dong, J. Hu, W. Gao, Capturing hormones and bisphenol A from water via sustained hydrogen bond driven sorption in polyamide microfiltration membranes, Water Res., 47 (2013) 197-208.

[79] S. Morales-Torres, L.M. Pastrana-Martinez, J.L. Figueiredo, J.L. Faria, A.M.T. Silva, Graphene oxide-P25 photocatalysts for degradation of diphenhydramine pharmaceutical and methyl orange dye, Appl. Surf. Sci., 275 (2013) 361-368.

[80] J. Mendret, M. Hatat-Fraile, M. Rivallin, S. Brosillon, Hydrophilic composite membranes for simultaneous separation and photocatalytic degradation of organic pollutants, Sep. Purif. Technol., 111 (2013) 9-19.